AFRL-VA-WP-TP-2007-302

ANALYSIS OF THE RECONFIGURABLE CONTROL CAPABILITIES OF A SPACE ACCESS VEHICLE (PREPRINT)

Michael W. Oppenheimer, Anhtuan D. Ngo, and William B. Blake

DECEMBER 2006

Approved for public release; distribution unlimited.

STINFO COPY

AIR VEHICLES DIRECTORATE
AIR FORCE MATERIEL COMMAND
AIR FORCE RESEARCH LABORATORY
WRIGHT-PATTERSON AIR FORCE BASE, OH 45433-7542

NOTICE AND SIGNATURE PAGE

Using Government drawings, specifications, or other data included in this document for any purpose other than Government procurement does not in any way obligate the U.S. Government. The fact that the Government formulated or supplied the drawings, specifications, or other data does not license the holder or any other person or corporation; or convey any rights or permission to manufacture, use, or sell any patented invention that may relate to them.

This report was cleared for public release by the Air Force Research Laboratory Wright Site (AFRL/WS) Public Affairs Office and is available to the general public, including foreign nationals. Copies may be obtained from the Defense Technical Information Center (DTIC) (http://www.dtic.mil).

AFRL-VA-WP-TP-2007-302 HAS BEEN REVIEWED AND IS APPROVED FOR PUBLICATION IN ACCORDANCE WITH ASSIGNED DISTRIBUTION STATEMENT.

*//Signature//

Michael W. Oppenheimer
Electronics Engineer
Control Design and Analysis Branch
Air Force Research Laboratory
Air Vehicles Directorate

//Signature//

Deborah S. Grismer
Chief
Control Design and Analysis Branch
Air Force Research Laboratory
Air Vehicles Directorate

//Signature//

JEFFREY C. TROMP
Senior Technical Advisor
Control Sciences Division
Air Vehicles Directorate

This report is published in the interest of scientific and technical information exchange, and its publication does not constitute the Government's approval or disapproval of its ideas or findings.

*Disseminated copies will show "//Signature//" stamped or typed above the signature blocks.

REPORT DOCUMENTATION PAGE

Form Approved
OMB No. 0704-0188

1. REPORT DATE *(DD-MM-YY)*	2. REPORT TYPE	3. DATES COVERED *(From - To)*
December 2006	Conference Paper Preprint	09/01/2006 – 12/01/2006

4. TITLE AND SUBTITLE
ANALYSIS OF THE RECONFIGURABLE CONTROL CAPABILITIES OF A SPACE ACCESS VEHICLE (PREPRINT)

5a. CONTRACT NUMBER
In-house

5b. GRANT NUMBER

5c. PROGRAM ELEMENT NUMBER
62201F

6. AUTHOR(S)
Michael W. Oppenheimer, Anhtuan D. Ngo, and William B. Blake

5d. PROJECT NUMBER
A03G

5e. TASK NUMBER

5f. WORK UNIT NUMBER
0B

7. PERFORMING ORGANIZATION NAME(S) AND ADDRESS(ES)

Control Design and Analysis Branch (AFRL/VACA)
Control Sciences Division
Air Vehicles Directorate
Air Force Materiel Command, Air Force Research Laboratory
Wright-Patterson Air Force Base, OH 45433-7542

8. PERFORMING ORGANIZATION REPORT NUMBER
AFRL-VA-WP-TP-2007-302

9. SPONSORING/MONITORING AGENCY NAME(S) AND ADDRESS(ES)

Air Vehicles Directorate
Air Force Research Laboratory
Air Force Materiel Command
Wright-Patterson Air Force Base, OH 45433-7542

10. SPONSORING/MONITORING AGENCY ACRONYM(S)
AFRL-VA-WP

11. SPONSORING/MONITORING AGENCY REPORT NUMBER(S)
AFRL-VA-WP-TP-2007-302

12. DISTRIBUTION/AVAILABILITY STATEMENT
Approved for public release; distribution unlimited.

13. SUPPLEMENTARY NOTES
Conference paper submitted to the Proceedings of the 2007 IEEE Aerospace Conference, published by IEEE.

 PAO Case Number: AFRL/WS 07-0097 (cleared January 16, 2007). Paper contains color.

14. ABSTRACT

Future access to space vehicles will be required to achieve a high level of safety and operability. In order to achieve these goals, integrated adaptive guidance and control can be used to recover a vehicle from off-nominal conditions, such as control effector failures, engine out, loss of engine gimbal, and so on. In this work, a preliminary configuration for a space access vehicle is defined. The vehicle contains five control surfaces, a bodyflap, two elevons, and two rudders. A guidance and control (G&C) design tool to rapidly assess the necessary control effort of the vehicle to track its flight trajectory is developed. Given the conceptual configuration and a desired trajectory for re-entry flight, this G&C tool provides an inner-loop feedback control law and outer-loop feedback guidance law to track the given trajectory. The inner-loop control law, based on dynamic inversion with a non-linear control allocator, is used to linearize the vehicle dynamics over its flight envelope and assign control tasks to the available control effectors to track the desired roll rate, pitch rate, and yaw rate. The outer-loop guidance law is based on a backstepping method. Assessment of the vehicle's ability to recover from control failures is conducted in this work for a nominal re-entry flight.

15. SUBJECT TERMS
Space Access Vehicle, Control Allocation, Guidance and Control

16. SECURITY CLASSIFICATION OF:			17. LIMITATION OF ABSTRACT:	18. NUMBER OF PAGES	19a. NAME OF RESPONSIBLE PERSON (Monitor)
a. REPORT	b. ABSTRACT	c. THIS PAGE			Michael W. Oppenheimer
Unclassified	Unclassified	Unclassified	SAR	16	19b. TELEPHONE NUMBER *(Include Area Code)* N/A

Standard Form 298 (Rev. 8-98)
Prescribed by ANSI Std. Z39-18

Analysis of the Reconfigurable Control Capabilities of a Space Access Vehicle

Michael W. Oppenheimer, Senior Member
Anhtuan D. Ngo
William B. Blake
Control Design and Analysis Branch
2210 Eighth St., Bldg. 146, Rm. 305
Wright-Patterson AFB, OH, USA
937-255-8490
michael.oppenheimer@wpafb.af.mil

Abstract— Future access to space vehicles will be required to achieve a high level of safety and operability. In order to achieve these goals, integrated adaptive guidance and control can be used to recover a vehicle from off-nominal conditions, such as control effector failures, engine out, loss of engine gimbal, and so on. In this work, a preliminary configuration for a space access vehicle is defined. The vehicle contains five control surfaces, a bodyflap, two elevons, and two rudders. A guidance and control (G&C) design tool to rapidly assess the necessary control effort of the vehicle to track its flight trajectory is developed. This tool can be used as part of the preliminary design cycle in configuration, trajectory planning, structural analysis, aerodynamic modelling, or control surface sizing. Given the conceptual configuration and a desired trajectory for re-entry flight, this G&C tool provides an inner-loop feedback control law and outer-loop feedback guidance law to track the given trajectory. The inner-loop control law, based on dynamic inversion with a non-linear control allocator, is used to linearize the vehicle dynamics over its flight envelope and assign control tasks to the available control effectors to track the desired roll rate, pitch rate, and yaw rate. The outer-loop guidance law is based on a backstepping method that transforms the trajectory-related flight path angle and desired bank angle into commands in roll rate, pitch rate, and yaw rate. Assessment of the vehicle's ability to recover from control failures is conducted in this work for a nominal re-entry flight. This assessment is used to provide inputs to configuration development to overcome any shortcomings in inner-loop reconfiguration capabilities.

TABLE OF CONTENTS

IEEEAC paper # , Version , Updated

1. INTRODUCTION

During the space access vehicle preliminary design process, it is necessary to quickly and economically assess the vehicle's ability to recover from control effector failures. This paper details a framework that efficiently incorporates the space access vehicle's stability, guidance, and control considerations into the initial configuration development. In this approach, a well-known, high-fidelity trajectory generator (Program to Optimize Simulated Trajectories), a fast aerodynamic data computation algorithm (Missile Datcom), and a robust, large flight envelope control law are integrated in the analysis and assessment process to evaluate vehicle performance in stability, guidance, and control.

POST (Program to Optimize Simulated Trajectories) is a trajectory computation program developed by NASA-Langley in the 1970's to support the Space Shuttle program. POST finds a user-defined optimal trajectory based upon a simulation model with performance and loading constraints. This optimal trajectory is a compromise between the ascent phase trying to maximize the payload delivered to orbit, the entry phase trying to limit re-entry aerodynamic heating and structural loads, and the approach phase trying to prepare the vehicle for a successful landing. The ascent phase ends at stage separation which is defined as a velocity of 7,000 feet per second, a flight path angle of 20 degrees, an angle of attack of 0 degrees, and an altitude higher than 160,000 feet. During this phase the vehicle is ascending rapidly, passing through the transonic sound barrier, and trying to reach stage separation criteria. The entry phase begins at stage separation and ends near the landing site which is defined to be an altitude greater than 15,000 feet and a velocity greater than Mach 0.3. During this phase, the vehicle typically experiences the peak heating, dynamic pressure, and normal loads because the vehicle is ballistic and aerodynamic controls are ineffective. In this phase the vehicle will descend at a constant angle of attack of 35 degrees and then perform a pull-up maneuver to

intercept a constant flight-path angle of 12 degrees.

The POST simulation model consists of a rocket engine model, an aerodynamic model, mass model, atmosphere model, and Earth gravity model. All of these models are combined to estimate the forces and moments exerted upon the vehicle over time. Typically, POST trajectories use three degrees of freedom to solve the optimization problem; therefore, losses due to trim effects are not considered and control effectors may not be sized appropriately. In some cases, vehicles may appear to ”close” (correctly sized in terms of required fuel and subsystems) that are actually not closed and may not be closeable (fuel and subsystem growth rate is too high). Therefore, accurate sizing makes six degree of freedom (6 DOF) simulations a vital part of the vehicle design process. Additionally, the 6 DOF simulations provide higher fidelity results that can be used to impact other subsystems such as the thermal protection system, main rocket engine thrust, and main propellant tank volume.

The aerodynamic data of the vehicle can be obtained from Missile Datcom[1], which is a tool to rapidly estimate the aerodynamics of a wide variety of vehicle configurations. The predictive accuracy of Missile Datcom is adequate for preliminary designs. Iterations on the vehicle configurations are inevitable since the ultimate shape of the vehicle will be dependent upon the subsystem being utilized, such as payload size, propulsion method, launch, and landing configurations. Once the optimal trajectory has been calculated by POST, for a given vehicle configuration having the aerodynamic properties indicated by Missile Datcom, the task of stabilizing the vehicle and tracking the optimal trajectory is carried out by a control law. The control law is designed for the entire flight envelope and can accommodate the drastic change in speed, altitude, and vehicle's mass properties during ascent and reentry. These changes in the flight environment result in substantial variations in aero-dynamic pressure, stagnation temperature, center of gravity, and moments of inertia. Furthermore, the launch vehicle is powered by a propulsion system during its ascent and, for a reusable vehicle, may be unpowered during re-entry. The vehicle's launch configuration and landing configuration may also be different from each other. The novel control law, in this work, seeks to stabilize the vehicle and track an optimal trajectory without the lengthy design process or a complicated control law gain scheduling that is traditionally required. The inputs to the inner-loop control law are the commanded roll rate p_{des}, commanded pitch rate q_{des}, and commanded yaw rate r_{des}. The guidance and control interface translates the bank angle command and angle of attack command into the commanded roll, pitch and yaw rates p_{des}, q_{des}, r_{des} respectively. Using the output of the control law, the vehicle designer can assess vehicle performance in tracking the desired trajectory and make modifications to its configuration, if necessary. The design process is shown in Fig. 1.

The main thrust of this paper is to develop the model and

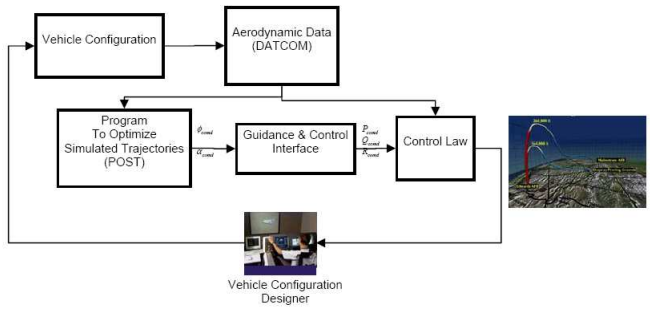

Figure 1. Space Access Vehicle's Preliminary Design Cycle

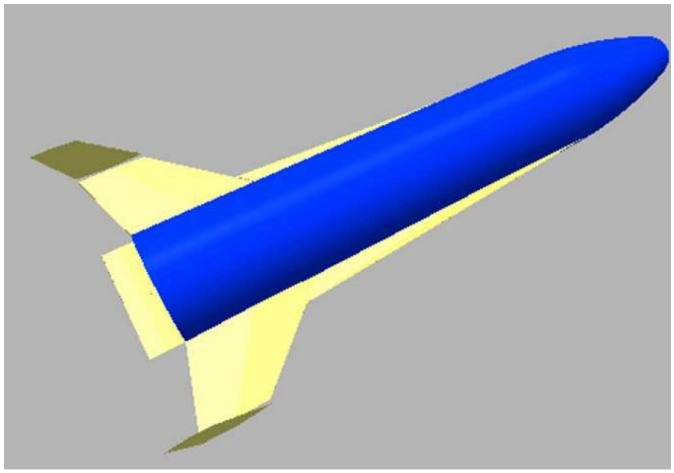

Figure 2. Preliminary Configuration for A Space Access Vehicle

control law and determine the ability of the vehicle to recover from locked control effector failures. In other words, to examine the inner-loop reconfiguration capabilities of the nominal vehicle. If the current suite of control effectors is not sufficient to recover from a wide range of locked effectors, the vehicle configuration/control effector suite can be modified to improve the reconfiguration capabilities.

2. VEHICLE MODELLING

The preliminary configuration for a baseline space access vehicle is shown in Fig. 2. The body, as modelled by Missile Datcom, consists of a blunted nose followed by a cylindrical afterbody with a 17 ft diameter. A single body flap was modelled at the base of the body. There was no modelling of external rocket nozzles. A straked wing with an outer panel sweep of 42° was modelled. Vertical tails were placed on each wingtip. Five control devices were modelled, two rudders (one on each vertical tail), two elevons (one on each wing) and a body flap. Missile Datcom was used to calculate the aerodynamic characteristics of the vehicle. Missile Datcom is a widely used engineering level code that uses the component buildup technique to predict vehicle characteristics. Code input consists of body, wing, and tail geometry,

Table 1. Space Access Vehicle Configuration Properties

Fuselage Length (feet)	**Wing Span** (feet)	**Weight** (pounds)	
102	42	65,474	
I_{xx} (slug-feet^2)	I_{yy} (slug-feet^2)	I_{zz} (slug-feet^2)	I_{xz} (slug-feet^2)
81,000	1,322,00	950,000	0

Mach number, altitude, angle of attack, and control deflections. Control devices are limited to all moving surfaces or plain trailing edge flaps. At each flight condition the six-body axis force and moment coefficients are provided. Both theoretical and empirical methods are included that encompass the entire speed regime from subsonic to hypersonic. Missile Datcom has been shown to provide very good agreement with experimental data for a variety of configurations. To validate the code for RLV type configurations, extensive comparisons have been made with wind tunnel data for the X-34 and X-40 configurations. Some of the X-34 comparisons are given by Ngo and Blake [2].

Moments of inertia for this vehicle were calculated using Eqs. 1, 2, and 3 obtained from Roskam [3].

$$I_{xx} = \frac{W}{g}(k_x\ b)^2 \quad (1)$$

$$I_{yy} = \frac{W}{g}(k_y\ l)^2 \quad (2)$$

$$I_{zz} = \frac{W}{g}(k_z\ \frac{b+l}{2})^2 \quad (3)$$

where b is the span and l is the length of the vehicle. The non-dimensional radii of gyration (k factors) were taken from an Air Force Research Laboratory database of re-entry vehicle designs such as the Space Shuttle, X-40, etc. Values used for k_x, k_y and k_z were 0.150, 0.25 and 0.30 respectively. This method does not give the product of inertia so this was assumed to be zero, that is, $I_{xz} = 0$, $I_{xy} = 0$, and $I_{yz} = 0$. The dimensions of the baseline space access vehicle design are summarized in Table 1. The control effectors limits are shown in Table 2.

3. DYNAMIC INVERSION

The purpose of the inner-loop control system is to accurately track body-frame angular velocity vector commands. The inner-loop control architecture developed in this work consists of three major components: a dynamic inversion control law, a control allocation algorithm, and precompensation.

Table 2. Space Access Vehicle Control Effectors

Control Effector	**Deflection Range**
Left Elevon	$\pm\ 30^\circ$
Right Elevon	$\pm\ 30^\circ$
Left Rudder	$\pm\ 30^\circ$
Right Rudder	$\pm\ 30^\circ$
Body Flap	$\pm\ 20^\circ$

The goal of dynamic inversion in flight control is to cancel the wing-body-propulsion forces and moments with control effector forces and moments such that the vehicle can accurately track some desired commands. Dynamic inversion control laws [4] require the use of a control mixer or control effector allocation algorithm when the number of control effectors exceeds the number of controlled variables, or when actuator rate and position limits must be taken into account. It is quite common that the desired control variable rate commands can be achieved in many different ways and so control allocation algorithms are used to provide unique solutions to such problems [5]. The control allocation algorithm is significantly improved by including an intercept term [6]. To complete the inner-loop, precompensation blocks are designed to produce the desired closed-loop dynamics. For the purpose of demonstration, we develop a dynamic inversion control law for a vehicle with five control surfaces. The control surfaces include two rudders, two elevons, and a bodyflap. An outer-loop control system generates body-frame angular velocity commands (p_{des}, q_{des}, r_{des}), that the inner-loop dynamic inversion control system attempts to track. The dynamics of the body-frame angular velocity vector for this vehicle can be written as

$$\dot{\boldsymbol{\omega}} = \mathbf{f}(\boldsymbol{\omega}, \mathbf{P}) + \mathbf{g}(\mathbf{P}, \boldsymbol{\delta}) \quad (4)$$

where $\boldsymbol{\omega}$ = [p q r]^T, p, q, and r are the rolling, pitching, and yawing rates, respectively, $\mathbf{P}$ is a vector of quantities that influence the body-frame states, and $\boldsymbol{\delta} = (\delta_1, \delta_2, \cdots, \delta_n)^T$ is a vector of control surface deflections. The vector $\mathbf{P}$ contains variables such as angle of attack, sideslip, Mach number, and vehicle mass properties. The term $\mathbf{g}(\mathbf{P}, \boldsymbol{\delta})$ includes the control dependent accelerations, while the term $\mathbf{f}(\boldsymbol{\omega}, \mathbf{P})$ describes accelerations that are due to the base-vehicle's (wing-body-propulsion) aerodynamic properties. The moment equations for a vehicle in the body-frame [7] can be manipulated to form control dependent and control independent

terms. It is assumed that the mass properties of the vehicle under consideration are constant, thus, the time derivative of the inertia matrix can be set to zero, i.e., $\dot{\mathbf{I}} = \mathbf{0}$. Then, Eq. 4 can be written as

$$\dot{\boldsymbol{\omega}} = \mathbf{I}^{-1}(\mathbf{G}_B(\boldsymbol{\omega}, \mathbf{P}, \boldsymbol{\delta}) - \boldsymbol{\omega} \times \mathbf{I}\boldsymbol{\omega}) \tag{5}$$

where

$$\mathbf{G}_B(\boldsymbol{\omega}, \mathbf{P}, \boldsymbol{\delta}) = \mathbf{G}_{BAE}(\boldsymbol{\omega}, \mathbf{P}) + \mathbf{G}_\delta(\mathbf{P}, \boldsymbol{\delta}) = \begin{bmatrix} L \\ M \\ N \end{bmatrix}_{BAE} + \begin{bmatrix} L \\ M \\ N \end{bmatrix}_\delta \tag{6}$$

In Eqs. 5 and 6, $\mathbf{I}$ is the inertia matrix and L, M, and N are the rolling, pitching, and yawing moments. In Eq. 6, $\mathbf{G}_{BAE}(\boldsymbol{\omega}, \mathbf{P})$ is the moment generated by the base aerodynamic system (wing-body-propulsion system) and $\mathbf{G}_\delta(\mathbf{P}, \boldsymbol{\delta})$ is the sum of moments produced by the control effectors. Therefore,

$$\begin{aligned} \mathbf{f}(\boldsymbol{\omega}, \mathbf{P}) &= \mathbf{I}^{-1}[\mathbf{G}_{\mathbf{BAE}}(\boldsymbol{\omega}, \mathbf{P}) - \boldsymbol{\omega} \times \mathbf{I}\boldsymbol{\omega}] \\ \mathbf{g}(\mathbf{P}, \boldsymbol{\delta}) &= \mathbf{I}^{-1}\mathbf{G}_\delta(\mathbf{P}, \boldsymbol{\delta}) \end{aligned} \tag{7}$$

In order to utilize a linear control allocator, it is necessary that the control dependent portion of the model be linear in the controls. Hence, an affine approximation is developed such that

$$\mathbf{G}_\delta(\mathbf{P}, \boldsymbol{\delta}) \approx \widetilde{\mathbf{G}}_\delta(\mathbf{P})\boldsymbol{\delta} + \boldsymbol{\epsilon}(\mathbf{P}, \boldsymbol{\delta}) \tag{8}$$

The term $\boldsymbol{\epsilon}(\mathbf{P}, \boldsymbol{\delta})$ is an intercept term [6] for the body-axis angular accelerations, which is used to improve the accuracy of linear control allocation algorithms. Using Eqs. 4, 7, and 8, the model used for the design of the dynamic inversion control law becomes

$$\dot{\boldsymbol{\omega}} = \mathbf{f}(\boldsymbol{\omega}, \mathbf{P}) + \mathbf{I}^{-1}\widetilde{\mathbf{G}}_\delta(\mathbf{P})\boldsymbol{\delta} + \mathbf{I}^{-1}\boldsymbol{\epsilon}(\mathbf{P}, \boldsymbol{\delta}) \tag{9}$$

The objective is to find a control law, that provides direct control over $\dot{\boldsymbol{\omega}}$, so that $\dot{\boldsymbol{\omega}} = \dot{\boldsymbol{\omega}}_{des}$. Hence, the inverse control law must satisfy

$$\dot{\boldsymbol{\omega}}_{des} - \mathbf{f}(\boldsymbol{\omega}, \mathbf{P}) - \mathbf{I}^{-1}\boldsymbol{\epsilon}(\mathbf{P}, \boldsymbol{\delta}) = \mathbf{I}^{-1}\widetilde{\mathbf{G}}_\delta(\mathbf{P})\boldsymbol{\delta} \tag{10}$$

Equation 10 provides the dynamic inversion control law for the body-frame angular velocity vector.

4. CONTROL ALLOCATION

Since there are more control effectors than controlled variables and the control effectors are restricted by position and rate limits, a control allocation algorithm is necessary. For the lifting body under consideration, there are three controlled variables, namely, roll, pitch, and yaw rates, while there are five control surfaces (left and right rudders, left and right elevators, and a bodyflap). Hence, a control allocation scheme must be used to ensure that Eq. 10 is satisfied.

Control allocators are used in conjunction with some type of feedback control law whose output consists of one or more pseudo-control commands (typically desired moment or acceleration commands). The number of pseudo-control commands is always less than or equal to the number of control effectors. Dynamic inversion control laws and control allocation algorithms fit together quite naturally since the pseudo-control commands are easily identifiable. Also, it is quite common that the desired commands can be achieved in many different ways and so control allocation algorithms are used to provide unique solutions to such problems.

To begin development of the allocator, rewrite Eq. 10 as

$$\mathbf{d}_{des} = \dot{\boldsymbol{\omega}}_{des} - \mathbf{f}(\boldsymbol{\omega}, \mathbf{P}) - \mathbf{I}^{-1}\boldsymbol{\epsilon}(\mathbf{P}, \boldsymbol{\delta}) = \mathbf{I}^{-1}\widetilde{\mathbf{G}}_\delta(\mathbf{P})\boldsymbol{\delta} = \mathbf{B}\boldsymbol{\delta} \tag{11}$$

where $\mathbf{d}_{des}$ are the body-axis accelerations that need to be produced by the control effectors and $\mathbf{B}$ is the control effectiveness matrix defined as

$$\mathbf{B} = \mathbf{I}^{-1}\widetilde{\mathbf{G}}_\delta(\mathbf{P}) = \mathbf{I}^{-1}\begin{bmatrix} \frac{\partial L}{\partial \delta_1} \frac{\partial L}{\partial \delta_2} \cdots \frac{\partial L}{\partial \delta_n} \\ \frac{\partial M}{\partial \delta_1} \frac{\partial M}{\partial \delta_2} \cdots \frac{\partial M}{\partial \delta_n} \\ \frac{\partial N}{\partial \delta_1} \frac{\partial N}{\partial \delta_2} \cdots \frac{\partial N}{\partial \delta_n} \end{bmatrix} \tag{12}$$

The control allocation objective, in the linear case, is to find $\boldsymbol{\delta}$ such that

$$\mathbf{d}_{des} = \mathbf{B}\boldsymbol{\delta} \tag{13}$$

subject to rate and position limits on the control effectors. Notice that Eq. 13 defines a linear subspace in the $(\mathbf{d}_{des}, \boldsymbol{\delta})$ space.

Equation 13 can be posed as the following optimization problem:

$$\min_{\delta} J_E = \min_{\delta} \|\mathbf{B}\boldsymbol{\delta} - \mathbf{d}_{des}\|_1 \tag{14}$$

subject to

$$\overline{\boldsymbol{\delta}} \leq \boldsymbol{\delta} \leq \underline{\boldsymbol{\delta}} \tag{15}$$

where J_E is the performance index for the error minimization problem, $\underline{\boldsymbol{\delta}}$, $\overline{\boldsymbol{\delta}}$ are the most restrictive lower and upper limits on the control effectors, respectively and the 1-norm is selected so that linear programming techniques can be used to solve the problem [8]. More specifically,

$$\begin{aligned} \overline{\boldsymbol{\delta}} &= \min(\boldsymbol{\delta}_U, \boldsymbol{\delta} + \dot{\boldsymbol{\delta}}\Delta t) \\ \underline{\boldsymbol{\delta}} &= \max(\boldsymbol{\delta}_L, \boldsymbol{\delta} - \dot{\boldsymbol{\delta}}\Delta t) \end{aligned} \tag{16}$$

where $\boldsymbol{\delta}_L, \boldsymbol{\delta}_U$ are the lower and upper position limits, $\boldsymbol{\delta}$ is the current location of the control effectors, $\dot{\boldsymbol{\delta}}$ is a vector of rate limits, and Δt is the timestep or control update rate.

If sufficient control authority exists such that J_E can be made identically equal to zero, then it may be possible to optimize a sub-objective. This optimization problem can be posed as follows:

$$\min_{\delta} J_C = \min_{\delta} \|\mathbf{W}_\delta(\boldsymbol{\delta} - \boldsymbol{\delta}_p)\|_1 \tag{17}$$

subject to

$$\begin{aligned} \mathbf{B}\boldsymbol{\delta} &= \mathbf{d}_{des} \\ \overline{\boldsymbol{\delta}} &= \min(\boldsymbol{\delta}_U, \boldsymbol{\delta} + \dot{\boldsymbol{\delta}}\Delta t) \\ \underline{\boldsymbol{\delta}} &= \max(\boldsymbol{\delta}_L, \boldsymbol{\delta} - \dot{\boldsymbol{\delta}}\Delta t) \end{aligned} \tag{18}$$

where $\mathbf{W}_\delta$ is a weighting matrix and $\boldsymbol{\delta}_p$ is a preferred set of control effector deflections. The problem posed in Eq. 17 is termed the control minimization problem.

In practice, the two optimization problems given in Eqs. 14 and 17 are combined to form what is known as the mixed optimization problem. The mixed optimization problem is defined as

$$\min_{\delta} J_M = \min_{\delta} \left(\|\mathbf{B}\boldsymbol{\delta} - \mathbf{d}_{des}\|_1 + \lambda \|\mathbf{W}_\delta(\boldsymbol{\delta} - \boldsymbol{\delta}_p)\|_1 \right) \tag{19}$$

where the parameter λ is used to weight the error and control minimization problems. For this work, it was determined that λ = 0.01 provided good error minimization while still driving the control effectors to the preferred values when sufficient control authority existed. The advantage of the mixed optimization problem is that it can often be solved faster and with better numerical properties as compared to sequentially solving the error and control minimization problems [5].

Control Allocation Preference Vector and Effector Failures

As specified in Eq. 19, a preference vector, $\boldsymbol{\delta}_p$, must be selected. One difficulty with the linear programming framework for solving the control allocation problem is that no model of the control allocator exists. This causes problems when performing linear stability analysis as there is no way to know the input/output relationship of the allocation algorithm. Fortunately, when sufficient control authority exists, the allocation algorithm will attempt to minimize the difference between the control deflections and a preferred set of control deflections. One obvious choice for preference vector is the pseudo-inverse solution. In this case, when sufficient control authority exists, the control allocation algorithm will drive the surfaces to the pseudo-inverse solution. Hence, in a robustness analysis, the control allocator can be replaced by the pseudo-inverse solution (assuming sufficient control authority exists). The pseudo-inverse solution is the two-norm solution to the control allocation problem and can be formulated as follows:

$$\min_{\boldsymbol{\delta}} \frac{1}{2}(\boldsymbol{\delta} + \mathbf{c})^{\mathbf{T}}\mathbf{W}(\boldsymbol{\delta} + \mathbf{c}) \tag{20}$$

subject to

$$\mathbf{B}\boldsymbol{\delta} = \mathbf{d}_{des} \tag{21}$$

where $\mathbf{W}$ is a weighting matrix and $\mathbf{c}$ is an offset vector. To solve this problem, first find the Hamiltonian (H) such that

$$\begin{aligned} H = \frac{1}{2}\boldsymbol{\delta}^T\mathbf{W}\boldsymbol{\delta} + \frac{\mathbf{1}}{\mathbf{2}}\mathbf{c}^{\mathbf{T}}\mathbf{W}\boldsymbol{\delta} + \\ \frac{1}{2}\boldsymbol{\delta}^T\mathbf{W}\mathbf{c} + \frac{\mathbf{1}}{\mathbf{2}}\mathbf{c}^{\mathbf{T}}\mathbf{W}\mathbf{c} + \boldsymbol{\xi}(\mathbf{B}\boldsymbol{\delta} - \mathbf{d}_{\mathbf{des}}) \end{aligned} \tag{22}$$

where $\boldsymbol{\xi} \in \mathbb{R}^{\aleph}$ is an as yet undetermined Lagrange multiplier. Taking the partial derivatives of H with respect to $\boldsymbol{\delta}$ and $\boldsymbol{\xi}$, setting these expressions equal to zero, and rearranging, gives

$$\begin{aligned} \frac{\partial H}{\partial \boldsymbol{\delta}} = \mathbf{W}\boldsymbol{\delta} + \frac{1}{2}(\mathbf{c}^{\mathbf{T}}\mathbf{W})^{\mathbf{T}} + \frac{\mathbf{1}}{\mathbf{2}}\mathbf{W}\mathbf{c} + (\boldsymbol{\xi}\mathbf{B})^{\mathbf{T}} = \mathbf{0} \\ \Longrightarrow \mathbf{W}\boldsymbol{\delta} = -\mathbf{W}\mathbf{c} - \mathbf{B}^{\mathbf{T}}\boldsymbol{\xi}^{\mathbf{T}} \end{aligned} \tag{23}$$

and

$$\begin{aligned} \frac{\partial H}{\partial \boldsymbol{\xi}} = \mathbf{B}\boldsymbol{\delta} - \mathbf{d}_{des} = \mathbf{0} \\ \Longrightarrow \mathbf{B}\boldsymbol{\delta} = \mathbf{d}_{des} \Longrightarrow \mathbf{B}\mathbf{W}^{-1}\mathbf{W}\boldsymbol{\delta} = \mathbf{d}_{des} \end{aligned} \tag{24}$$

Substituting Eq. 23 into Eq. 24 yields

$$\mathbf{B}\mathbf{W}^{-1}[-\mathbf{W}\mathbf{c} - \mathbf{B}^T\boldsymbol{\xi}^T] = \mathbf{d}_{des} \tag{25}$$

Solving for $\boldsymbol{\xi}^T$ in Eq. 25 yields

$$\boldsymbol{\xi}^T = -(\mathbf{B}\mathbf{W}^{-1}\mathbf{B}^T)^{-1}[\mathbf{d}_{des} + \mathbf{B}\mathbf{c}] \tag{26}$$

Substituting Eq. 26 into Eq. 23 produces

$$\mathbf{W}\boldsymbol{\delta} = -\mathbf{W}\mathbf{c} + \mathbf{B}^T(\mathbf{B}\mathbf{W}^{-1}\mathbf{B}^T)^{-1}[\mathbf{d}_{des} + \mathbf{B}\mathbf{c}] \tag{27}$$

Simplifying Eq. 27 gives the desired result

$$\boldsymbol{\delta} = \boldsymbol{\delta}_p = -\mathbf{c} + \mathbf{W}^{-1}\mathbf{B}^T(\mathbf{B}\mathbf{W}^{-1}\mathbf{B}^T)^{-1}[\mathbf{d}_{des} + \mathbf{B}\mathbf{c}] \tag{28}$$

Equation 28 gives the pseudo-inverse solution. It should be noted that if an effector is offset, two items must be taken into account, position offset ($-\mathbf{c}$) and the moments generated by the offset ($\mathbf{B}\mathbf{c}$). For the specific usage of the pseudo-inverse control allocation solution, the weighting matrix was selected to be diagonal, such that,

$$\mathbf{W} = \mathbf{diag}\left[\mathbf{W}_{\delta_{\mathbf{RF}}}\ \mathbf{W}_{\delta_{\mathbf{LF}}}\ \mathbf{W}_{\delta_{\mathbf{RR}}}\ \mathbf{W}_{\delta_{\mathbf{LR}}}\ \mathbf{W}_{\delta_{\mathbf{SB}}}\ \mathbf{W}_{\delta_{\mathbf{BF}}}\right] \tag{29}$$

where 'diag' represents a diagonal matrix with the entries along the main diagonal being the weights associated with each control effector.

This control allocation formulation allows one to simulate a control effector failure rather easily. A failure is introduced by simply setting the lower and upper positions limits on the effected control surface equal to each other. For a failed control surface, its effects must also be accounted for in the pseudo-inverse preference vector, which requires two modifications. First, the location of the failure must be inserted into the offset vector. Here, the appropriate component of $\mathbf{c}$ is set to the negative of the failure position. Second, the appropriate entry in the weighting matrix, $\mathbf{W}$, needs to be increased. Nominally, the entries in $\mathbf{W}$ are one and an increase in the value will place more penalty on usage of that particular surface.

Figure 3 shows the inner-loop control law block diagram. The dynamic inversion control law is formed at a summing junction followed by allocation of control effector commands. A

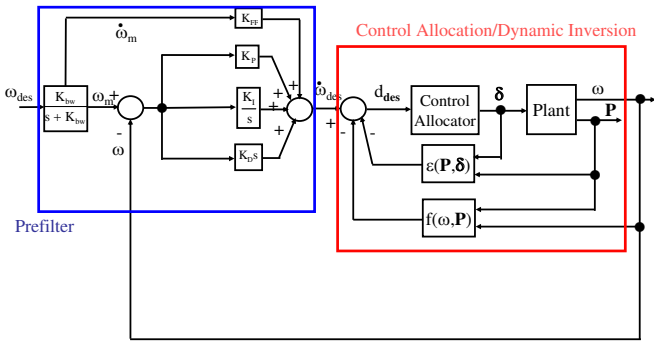

Figure 3. Inner-Loop Control Law Block Diagram.

part of the control law not covered in this work is the prefilter. The prefilter is used to shape the dynamic response of the system and to provide robustness. Here, a first-order explicit model following prefilter is used so that, under perfect conditions, the roll, pitch, and yaw rate signals act like the outputs of first-order lag transfer functions.

5. Guidance Loops

The guidance loops developed in this work have as inputs angle of attack error α_e and euler angle phi error ϕ_e and provide as outputs the commanded roll, pitch, and yaw rates. A backstepping approach is used to move from the angle of attack and phi loops to the body-axis rate loops.

To derive the pitch rate command, the governing equation of motion is

$$\gamma = \theta - \alpha \tag{30}$$

Therefore,

$$\dot{\alpha} = \dot{\theta} - \dot{\gamma} \tag{31}$$

By definition,

$$\dot{\theta} = q\cos\phi - r\sin\phi \tag{32}$$

and

$$\dot{\gamma} = \frac{L}{mV} - \frac{g}{V}\cos\gamma \tag{33}$$

where L is the total vehicle lift, m is the mass, V is the velocity, and g is the acceleration due to gravity. Substituting Eqs. 32 and 33 into Eq. 31 yields

$$\dot{\alpha} = q\cos\phi - r\sin\phi - \frac{L}{mV} + \frac{g}{V}\cos\gamma \tag{34}$$

From dynamic inversion, the pitch rate command becomes

$$q_{des} = \sec\phi\left(\dot{\alpha}_{des} + r\sin\phi + \frac{L}{mV} - \frac{g}{V}\cos\gamma\right) \tag{35}$$

The desired angle of attack dynamics are defined by the following proportional-integral control on α error:

$$\dot{\alpha}_{des} = \left(k_{p_\alpha} + \frac{k_{i_\alpha}}{s}\right)(\alpha_{des} - \alpha) \tag{36}$$

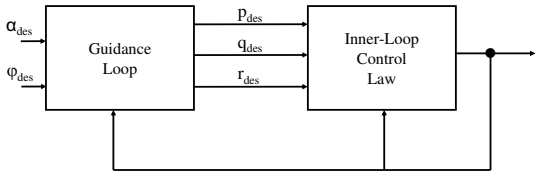

Figure 4. Guidance and Inner-Loop Control Law Interfaces.

For the lateral channels, the roll rate command is simply the result of a proportional-integral operation on phi error. Thus,

$$p_{des} = \left(k_{p_\phi} + \frac{k_{i_\phi}}{s}\right)(\phi_{des} - \phi) \tag{37}$$

From the coordinated turn equations, the yaw rate command is computed using

$$r_{des} = p\tan\alpha + \frac{g}{U}\sin\phi \tag{38}$$

Equations 37, 35, and 38 define the commanded or desired body axis rates generated from errors between the actual and desired angle of attack α_{des} and desired roll angle ϕ_{des}.

Figure 4 shows the interface between the guidance and inner-loop control laws. The guidance loop takes α_{des} and ϕ_{des} as inputs and produces commands to the inner-loop in the form of p_{des}, q_{des}, and r_{des}. The inner-loops' task is to then track these body-axis angular rates. The feedback lines represent the numerous variables that each loop requires.

6. Nominal Simulation Results

In this section, we will use the above aforementioned methods to simulate a guidance and control law for the nominal vehicle. Given a re-entry trajectory, a POST simulation outputs the desired angle of attack α_{des} and desired roll angle ϕ_{des} as part of its calculations. A guidance law based on the backstepping method discussed in section 5 is designed to convert the desired angle of attack α_{des} and desired roll angle ϕ_{des} into the commanded roll rate p_{des}, the commanded pitch rate q_{des} and the commanded yaw rate r_{des}. The commanded body-axis rates p_{des}, q_{des}, r_{des}, in turn, are converted into required control deflections by the dynamic-inversion control law mentioned in section 3. A control allocator based on the discussion in section 4 assigns the required control deflections over the control effectors according to their available capabilities. The tracking performance of the control law, under nominal conditions, is shown in Fig. 5. Tracking errors $p_{des} - p_{actual}$, $q_{des} - q_{actual}$, $r_{des} - r_{actual}$ are small. These small errors are desired and expected since our design method is formulated to directly track p_{des}, q_{des}, r_{des}. The commanded and actual Euler angles are shown in Fig. 6. Tracking of ϕ is excellent since this variable is directly used in the guidance loops. Since the control law does not explicitly attempt to track θ or ψ, it is expected that tracking errors

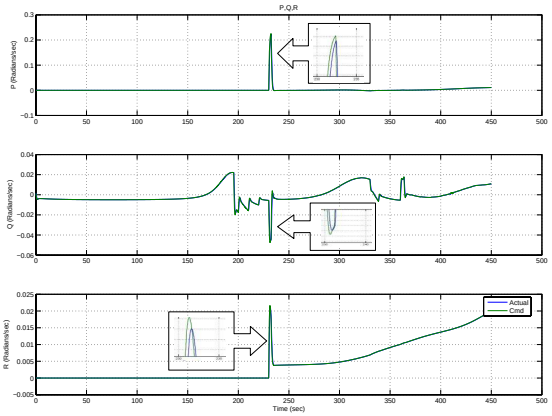

Figure 5. Roll Rate, Pitch Rate, and Yaw Rate Tracking

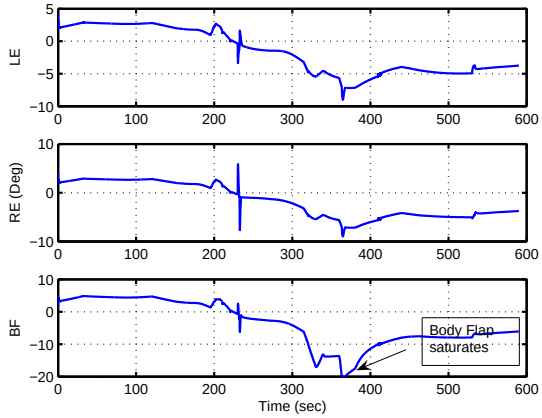

Figure 7. Left Elevon, Right Elevon, Body Flap Deflections

]

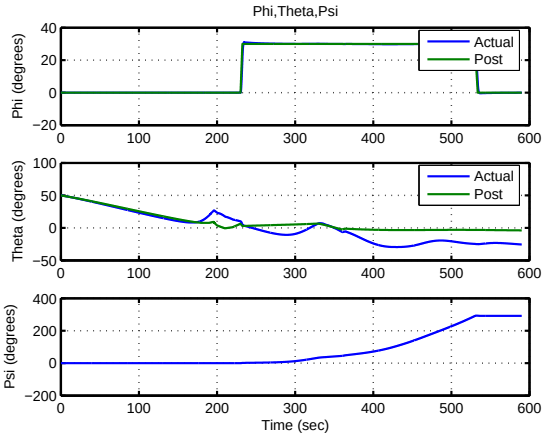

Figure 6. Rolling Angle, Pitch Angle, and Yaw Angle Tracking

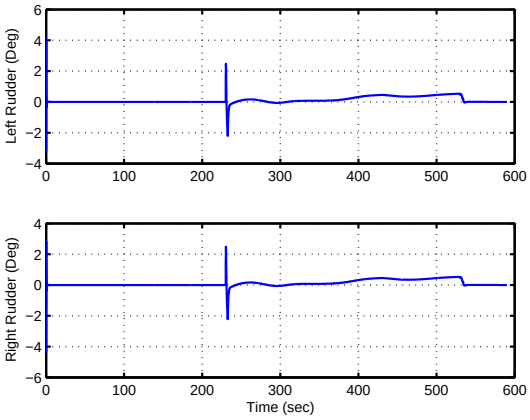

Figure 8. Left Rudder and Right Rudder Deflections

will exist in these time histories. In Figs. 7 and 8, the control deflection activities of the left elevon, right elevon, left rudder and right rudder are reasonable without exceeding its rate and position limits. It is noted, however, that the pitch flap briefly saturates at its deflection limit. Figure 9 shows the velocity, angle of attack, sideslip angle, and flight-path angle time histories. Angle of attack tracking is very good, as expected, since α is a variable which is directly tracked by this control law.

7. Inner-Loop Reconfiguration Simulation Results

In this section, the ability of the vehicle to recover from locked control effectors is examined. Only one of the left/right pair of effectors is failed and the assumption is made that the same ability to recover the vehicle exists for the other effector in the pair (due to symmetry). Even though the tra-

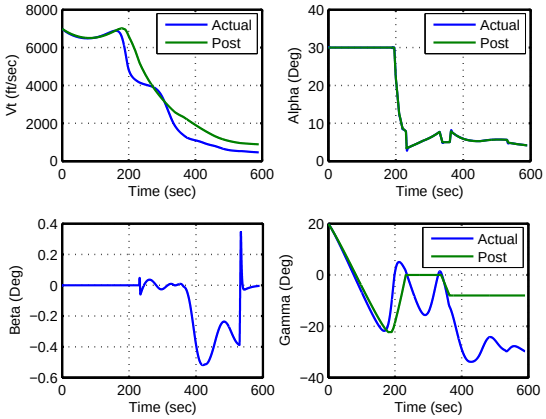

Figure 9. Velocity, Angle of Attack, Side Slip Angle, and Flight Path Angle Tracking

jectory does not specify wings-level flight, assuming the same recovery ability exists for a symmetric pair of effectors is sufficient for this stage of the work. It should also be pointed out that the range of recoverable failures is highly dependent on the initial conditions and trajectory selected for flight. In order to make a definitive statement about the control reconfiguration capabilities, more work would need to be performed, utilizing different initial conditions and trajectories. The work presented here is a first cut at evaluating the control reconfiguration capabilities of this vehicle.

To begin, failure of a single elevon is considered. The range of recoverable elevon failures is about -10° to -5° for the nominal re-entry profile in this work. Figures 10 and 11 show the body-axis rate tracking for a failed left elevon at -10° and -13°. When the left elevon is failed at -10°, the vehicle can recover and near nominal performance is achieved using reconfigurable inner-loop control (see Fig. 10). Here, starting at about 360 seconds, there is a period of poor pitch rate tracking. This is directly attributable to the bodyflap saturating for about 40 seconds. At about 400 seconds, the bodyflaps moves off of its position limit and quality pitch rate tracking returns. When the failure occurs at -13°, the vehicle can no longer track the nominal commands, as seen by the divergence in pitch rate tracking in Fig. 11.

For rudder failures, a large envelope of recoverable failures exists. In fact, the vehicle can tolerate left or right rudder failure between -23° and 26° (nearly the entire deflection range).

In terms of reconfigurable control, the current bodyflap is problematic. The vehicle cannot tolerate a failure of the bodyflap at any location and Fig. 12 shows the roll, pitch, and yaw rate tracking for the bodyflap failed at 0°. The bodyflap is the primary pitching moment device and without it, the vehicle cannot simultaneously produce the required rolling, pitching, and yawing accelerations. In light of the issues with recovering from bodyflap failures, a configuration redesign for the vehicle is necessary. One way to alleviate this issue is to split the bodyflap into two independent devices, a left/right pair. Essentially, this adds redundancy to the pitching moment capabilities of the vehicle. Now, when one of the bodyflap pair fails, the vehicle can recover nominal performance. Figure 13 shows the roll, pitch, and yaw rate tracking when the left bodyflap is failed at 0°. Clearly, the vehicle has recovered nominal performance and by splitting the bodyflap into two devices, additional redundancy has been included. Figures 14 and 15 show the control effector deflections for this case. Here it can be seen that the left bodyflap is at 0° for the entire simulation run while the right bodyflap is free to move.

Since the elevons have a relatively small range of failures for which nominal performance can be recovered, a future configuration change to the vehicle would be to split the elevons, much like the bodyflap. Splitting control effectors into two or more independent devices increases the control redundancy. The downside to this is that complexity and weight of the vehicle most likely increases, i.e., more actuators and hardware are necessary.

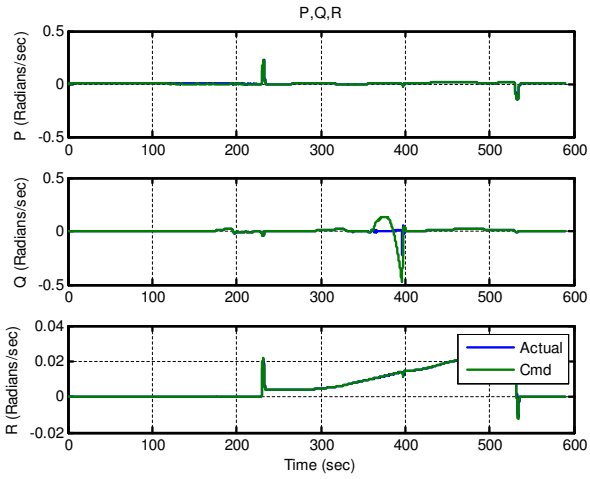

Figure 10. Roll, Pitch, and Yaw Rates vs. Time for Failed Left Elevon at -10°.

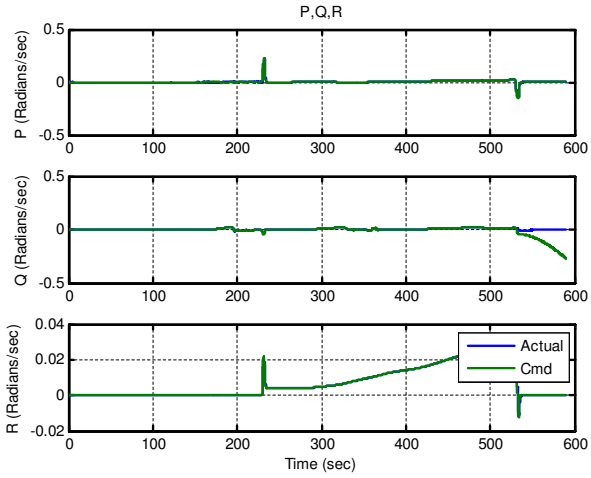

Figure 11. Roll, Pitch, and Yaw Rates vs. Time for Failed Left Elevon at -13°.

8. Conclusions

In this work, a rapid assessment tool for space access vehicle configurations in guidance and control performance was presented. The re-entry trajectory was found using a well-known, high-fidelity trajectory generator. To track this trajectory, an inner-loop, reconfigurable control law was designed for a re-entry vehicle with five control surfaces. The control law utilized a dynamic inversion controller and a linear programming based control allocation algorithm. Evaluation of the vehicle's ability to recover from failures showed that a small range of single elevon failures were recoverable, a

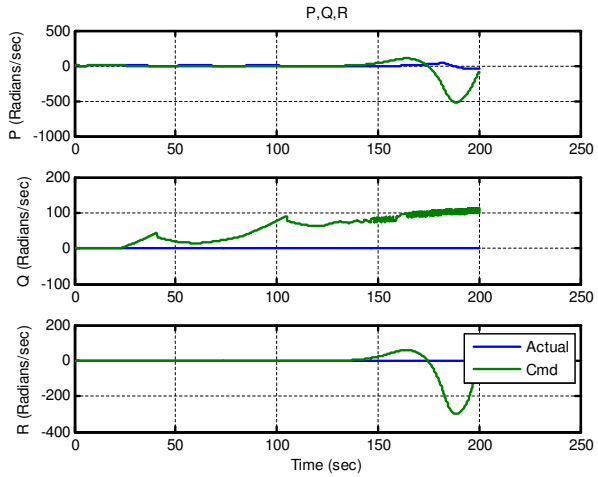

Figure 12. Roll, Pitch, and Yaw Rates vs. Time for Failed BodyFlap at 0°.

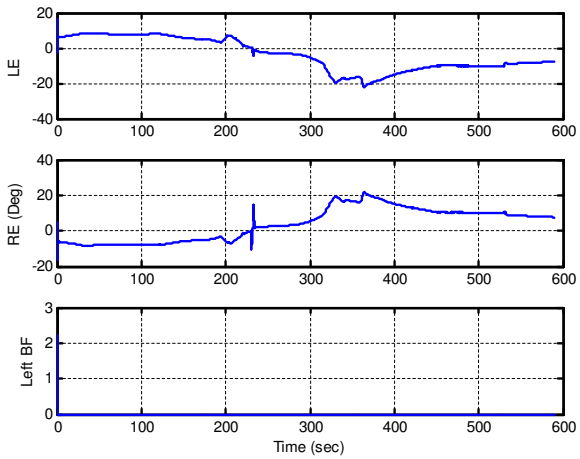

Figure 14. Left Elevon, Right Elevon, and Left BodyFlap vs. Time. Split BodyFlap. Failed Left BodyFlap at 0°.

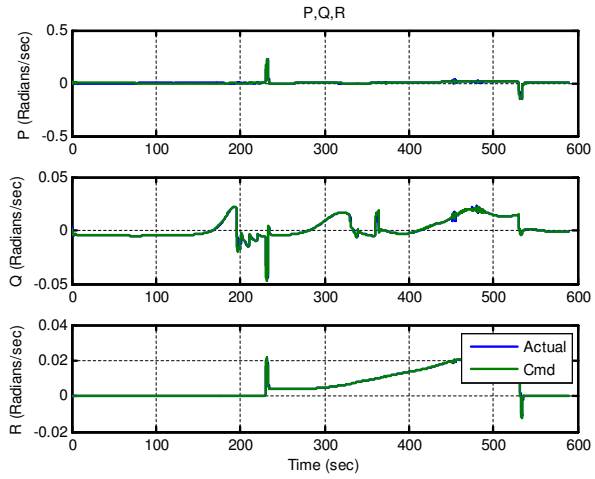

Figure 13. Roll, Pitch, and Yaw Rates vs. Time. Split BodyFlap. Failed Left BodyFlap at 0°.

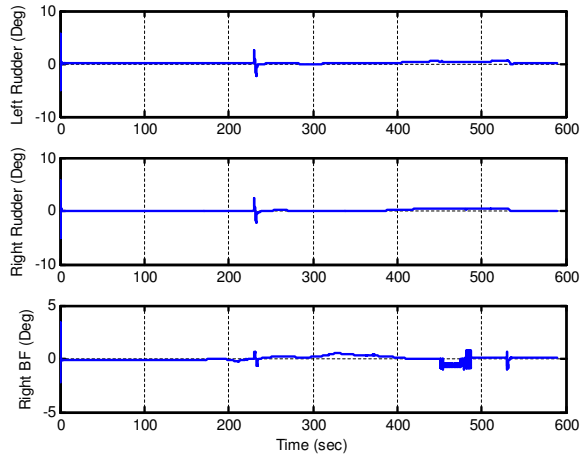

Figure 15. Left Rudder, Right Rudder, and Right BodyFlap vs. Time. Split BodyFlap. Failed Left BodyFlap at 0°.

large range of single rudder failures were recoverable, and no bodyflap failures were recoverable. It was thus necessary to consider modifications to the vehicle such as splitting the bodyflap into two control effectors. After splitting the bodyflap into a left/right pair, the vehicle could then tolerate a single bodyflap failure. Using the tool detailed in this paper, such modifications of the vehicle can be accommodated during the early design stages to incorporate the guidance and control requirements.

REFERENCES

[1] W. Blake, "Missile Datcom User's Manual - 1997 FORTRAN 90 Revision", Air Force Research Laboratory, WPAFB, OH, VA-WP-TR-1998-3009, August 1998.

[2] A. Ngo and W. Blake, "Longitudinal Control and Footprint Analysis for a Reusable Military Launch Vehicle", *Proceedings of the 2003 AIAA Guidance Navigation and Control Conference*, AIAA 2003-5738, August 2003.

[3] J. Roskam, *Airplane Design*, Roskam Aviation & Engineering Corporation, 1989.

[4] "Application of Multivariable Control Theory to Aircraft Control Laws", Wright Laboratory, WPAFB, OH, WL-TR-96-3099, 1996.

[5] M. Bodson, "Evaluation of Optimization Methods for Control Allocation", *Journal of Guidance, Control and Dynamics*, Volume 25, No. 4, 2002, pp. 703-711.

[6] D. Doman and M. Oppenheimer, "Improving Control Allocation Accuracy for Nonlinear Aircraft Dynamics", *Proceedings of the 2002 Guidance, Navigation and*

Control Conference, AIAA 2002-4667, August 2002.

[7] B. Etkin, *Dynamics of Atmospheric Flight*, John Wiley & Sons, Inc., 1972.

[8] J. Buffington, "Modular Control Law Design for the Innovative Control Effectors (ICE) Tailless Fighter Aircraft Configuration 101-3", Air Force Research Laboratory, WPAFB, OH, AFRL-VA-WP-TR-1999, 1999.

Michael Oppenheimer *Michael W. Oppenheimer is an Electronics Engineer at the Control Design and Analysis Branch at the Air Force Research Laboratory, Wright Patterson Air Force Base, OH. He is the author or co-author of more than 30 publications including refereed conference papers, journal articles, and a technical report. He holds a Ph. D. degree in Electrical Engineering from the Air Force Institute of Technology and is a member of AIAA and a senior member of IEEE. Dr. Oppenheimer's research interests are in the areas of nonlinear and adaptive control, including reconfigurable flight control and control allocation, and the application of this technology to air vehicles.*

Anhtuan D. Ngo *Anhtuan D. Ngo is a Control Engineer at the U.S. Air Force Research Laboratory. He is currently working in the area of Guidance and Control Space Access Vehicle. He received his B.S degree from Texas A& M University in 1992 and M.S.and Ph.D. degrees from University of Washington in 1995 and 2000 respectively. In the past three years, he worked as a control research engineer at the Air Force Research Laboratory / Air Vehicles Directorate, Dayton, Ohio. His research interests and publications were in analysis and design of nonlinear adaptive control system for aerospace vehicles, system identification and control allocation.*

William Blake *William B. Blake is an Aerospace Engineer at the Control Design and Analysis Branch at the Air Force Research Laboratory, Wright Patterson Air Force Base, OH. He is the author or co-author of more than 50 publications including refereed conference papers, journal articles, and technical reports. He holds an M.S degree in Aerospace Engineering from the University of Dayton and is an Associate Fellow of AIAA. Mr. Blake's research interests are in the areas of aerodynamics, stability and control, and flight mechanics.*